NOVA SCHOOL OF SCIENCE & TECHNOLOGY

DEPARTMENT OF MATERIALS SCIENCE

Guilherme Lopes Costa Ferreira

Master of science in
Micro and Nanotechnologies Engineering

Optimization of $MAPbI_3$-films grown under ambient conditions on Si/SiO_2 substrates for electrical characterization of perovskite materials

Msc Micro and Nanotechnologies Engineering

NOVA University Lisbon

October, 2022

NOVA SCHOOL OF
SCIENCE & TECHNOLOGY

DEPARTAMENT OF
MATERIALS AND SCIENCE

Optimization of $MAPbI_3$-films grown under ambient conditions on Si/SiO_2 substrates for electrical characterization of perovskite materials

Guilherme Lopes Costa Ferreira

Msc Micro and Nanotechnologies Engineering

Adviser: Dr. Iñigo Ramiro González
Post-Doc Fellow, School of Science and Technology – NOVA University of Lisbon

Co-adviser: Dr. Manuel J. Mendes,
Assistant Professor, School of Sciences and Technology – NOVA University of Lisbon

Examination Committee:

Chair: Dr. Hugo Manuel Brito Águas
Associate Professor, School of Science and Technology – NOVA University of Lisbon

Rapporteur: Dr. Jana Santanu,
Post-Doc Fellow, School of Science and Technology – NOVA University of Lisbon

Adviser: Dr. Iñigo Ramiro González
Post-Doc Fellow, School of Science and Technology – NOVA University of Lisbon

Members: Dr. Manuel J. Mendes,
Assistant Professor, School of Sciences and Technology – NOVA University of Lisbon

MASTER IN MICRO AND NANOTECHNOLOGIES ENGINEERING

NOVA University Lisbon
October, 2022

Optimization of $MAPbI_3$-films grown under ambient conditions on Si/SiO_2 substrates for electrical characterization of perovskite materials

ACKNOWLEDGMENTS

Primeiramente, gostaria de agradecer ao Professor Rodrigo Martins e a Professora Elvira Fortunato e a todos os envolvidos na criação e gestão do curso de MIEMN no qual tive a oportunidade de estudar nestes 5 anos. Quero também agradecer ao Professor Mendes por me ter conectado com o mundo dos fotovoltaicos e pelo envolvimento neste projeto de dissertação ao qual estou grato de ter feito parte.

I want to give special thanks to my thesis supervisor Dr. Iñigo not only for being the proponent of this thesis but also for the knowledge shared and allowing me to understand better how the scientific world works. I also want to extend these sentiments to Dr. Deneb for all of the help, availability and input inside and outside the lab. This thesis could not be done without both of you, and I am very thankful for all the help and motivation during this project.

Adiciono a estes agradecimentos a alguns jovens não tão importantes, mas que existem, não me largaram e estão presentes em mais memórias do que deviam durante estes 5 anos. À Catarina, por ser minha fiel seguidora, ao Taco por ser meu fiel contrário em tudo menos no humor, ao André por chegar atrasado a todos os compromissos juntos e ao Miguel por ter vivenciado a lenda do #Matlab comigo e espalhado tal lenda pelas ruas da Europa. A todas as pessoas que interagi ao longo do curso, obrigado.

Á minha namorada, Mádá, por toda a ajuda, paciência, vontade de ouvir e por ter sido a minha consistência no meio destes caóticos 5 anos onde tudo mudou menos ela.

Por fim, á minha família, por garantir e lutar para que nada me faltasse durantes o meu percurso universitário todo, muitas vezes mais difícil que fácil. Pela paciência para os meus estranhos horários de estudo e por serem a razão principal de acabar este curso e etapa. Obrigado.

“No great discovery was ever made without a bold guess.”
Isaac Newton

ABSTRACT

Perovskite materials have recently emerged as a family of potential semiconductor materials for the fabrication of optoelectronic devices such as solar cells, light-emitting diodes, and transistors.

This thesis aims to expand the available deposition and characterization techniques of the perovskite materials used by the research group I integrated. This allowed for the extraction of the doping character (n or p) of the perovskite layers deposited. To this end the deposition of $MAPbI_3$ (MAPI) perovskite material on an Si/SiO_2 substrate was thoroughly researched and optimized based on morphological, structural, and optical characterization. For that, different solutions, annealing methods and spin-coating parameters were tested and analyzed with the help of characterization tools like SEM, XRD, UV-vis and PL.

The film deposition was done under ambient conditions with the aim of allowing this characterization and deposition method to be made without more expensive equipment like the glovebox, where these materials are usually deposited, due to the controlled atmosphere conditions.

The MAPI films showed a small number or nonexistence of pinholes with good coverage across the film. PL and UV-vis measurements revealed a 1.59 eV band gap. The devices showed a field effect mobility of $1.5 \cdot 10^{-6}$ $cm^2/V.s$. At lower temperature, the devices improved, and the mobility extracted was $6.1 \cdot 10^{-5}$ $cm^2/V.s$.

Keywords: perovskite material; transistor; $MaPbI_3$, perovskite characterization

RESUMO

Materiais de perovskite têm surgido como potencias candidatos ao fabrico de dispositivos optoelectrónicos como células solares, díodos emissores de luz e transístores.

Esta tese pretende expandir as técnicas de deposição e caracterização dos materiais de perovskite usados pelo grupo de pesquisa integrado. Para esse fim, a deposição da perovskite $MAPbI_3$ (MAPI) em um substrato de Si/SiO_2 foi totalmente analisada e otimizada baseado em caracterização morfológica, estrutural e ótica. Para isso, soluções diferentes, métodos de recozimento e parâmetros de spin-coating foram testados e analisados com a ajuda de ferramentas de caracterização como SEM, XRD, UV-vis, e PL.

A deposição do filme foi feita sobre condições ambientes com o intuito de permitir a caracterização e deposição destes materiais sem a necessidade de equipamento mais caro como uma *glove-box*, onde estes materiais são usualmente depositados devido as condições atmosféricas controladas que o equipamento permite.

Os filmes de MAPI mostraram boa cobertura com a inexistência de buracos ao longo do filme. Medições de PL e UV-vis revelaram um hiato energético de 1.59 eV. Os dispositivos demonstraram uma mobilidade de efeito de campo de $1.5 \cdot 10^{-6}$ $cm^2/V.s$. A temperaturas mais baixas, os dispositivos melhoraram e mostraram uma mobilidade de $6.1 \cdot 10^{-5}$ $cm^2/V.s$.

Palavras-chave: materiais de perovskite; transístor; $MaPbI_3$; caracterização de perovskite

CONTENTS

LIST OF FIGURES

LIST OF TABLES

ACRONYMS

ABX_3 - Perovskite Structure
CB - Conduction Band
DMF - Dimethylformamide
DMSO - Dimethyl Sulfoxide
FET - Field Effect Transistor
FWHM - Full Width Half Maximum
GBL - gamma-Butyrolactone
IPA - Isopropyl Alcohol
LED - Light Emitting Diode
MA -Methylammonium
MAPI – $MAPbI_3$
PL - Photoluminescence
PbI_2 - Lead Iodide
SEM - Scanning Electron Microscopy
UV - Ultraviolet
UV-VIS - Ultraviolet-visible
VB – Valence Band

SYMBOLS AND UNITS

cm - Centimeter

K - Kelvin

min - Minute

nm - Nanometer

Rpm – Rotations per minute

μm – Micrometer

μA - Microampere

μL – Microliter

V - Volts

eV - Electronvolt

mV - Milivolts

mbar - Milibar

nA - Nanoampere

s - Second

°C – degree Celsius

λ – Wavelength

1

INTRODUCTION

1.1 Background and motivations

Solar energy continues to be studied at an increasing rate as the need for more efficient and more renewable ways of harvesting energy also increases. From the countless research, perovskite solar cells appeared as a material with great potential. One of the types of perovskites that is a focus for these studies is the organic-inorganic hybrid perovskite due to its inherent properties like high absorption coefficient, high diffusion lengths and high luminescence efficiency. Furthermore, the possibility of being solution-processed with simple deposition methods like spin-coating or drop-casting also adds to the reasons for the intensive investigation of these materials[1]–[3]. These properties that made perovskites attractive for the study of solar cells were also behind the reason for its application in other optoelectronic devices like LEDs, transistors, and phototransistors.

Even though perovskite materials can be easily solution processed, there are problems with stability and degradation when in contact with air [4]. Because of this, most perovskite devices are deposited under controlled atmosphere conditions using a glovebox, for example. This can hinder one of the main advantages for using these materials with simple deposition methods since it requires extra equipment. As such, one of the aims of this work is to optimize the deposition of $MAPbI_3$ for deposition in ambient conditions.

However, there remains a lot of properties to be studied and understood so that these materials can be properly applied in optoelectronics technology. Following such need, this study aims to understand the influence and impact of the steps in spin-coating deposition of the halide perovskite $MAPbI_3$. Furthermore, the deposition was made on SiO_2 so as to permit transistor fabrication. Through the deposited films and the fabricated transistor devices, an electrical and optical characterization of the material was made. This allowed for the extraction of properties like the doping type of the material, mobility, and band gap. This information will be useful for the research group as it will give information in the deposition and characteristics of these materials.

1.2 Overview of perovskite materials

A perovskite material is, by definition, considered a crystal structure that follows the formula of ABX_3. In this structure, A represents larger organic cations, B represents smaller metallic cations and X is represented by halide anions [5], [6]. These materials have interesting properties for like a tunable band gap, high absorption coefficient and long charge diffusion length [7]. Additionally, there is the potential for easier fabrication due to the materials being solution-processable and having low crystallization temperature. Due to said properties, perovskite materials attracted a lot of attention in the study of optoelectronic devices like LEDs, solar cell devices and FETs [6]. While the properties mentioned are characteristic of all perovskite materials, these properties can change by changing the cations of the material, leading to the existence of various types of perovskites that offer different results when applicated in optoelectronic devices [5]. One of the perovskite types that has received intensive research is the halide perovskite $CH_3NH_3PbI_3$ (MAPI), which will be the studied material in this thesis.

1.2.1 Crystal structure

MAPI crystal structure, band gap and other electrical properties can vary according to its phase. Phase transitions occur due to changes in temperature. At 330 K or higher MAPI presents an α phase, a cubic structure characterized for the random orientation of the molecules. At a temperature lower than 330 K, in the β phase, the structure is tetragonal, and the molecules show less freedom of movement but are still disorientated. At 165 K is the transition temperature for the γ phase, the orthorhombic structure. In this phase, the molecules are fixed [1]. There is also an amorphous δ phase which happens when the bond between B-X ions is broken.

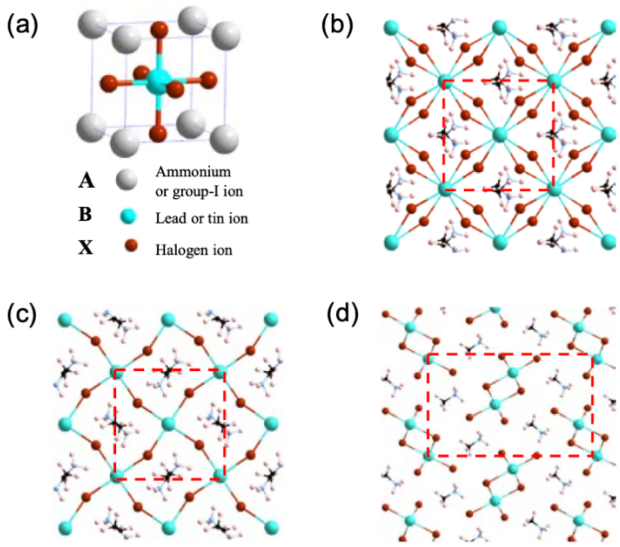

Figure 1 – Atomic structure for α phase (a), β phase (b), γ phase (c), δ phase (d) of MAPI [1].

The changes in structure with the temperature is related with the rotation of the C-N bond of the MA cation. There are also reports on an amorphous phase of MAPI where half of PbI_2 is not converted in MAPI. These phase transitions are important as they can influence band gap energy, electronic properties, and stability [8].

1.2.2 Electronic properties

Electronic properties of MAPI perovskite are one of the main reasons the material attracted attention on the optoelectronic field [1], [6], [9], [10]. From these properties, high diffusion lengths and low exciton binding energy are standouts for these devices. The low exciton binding energy is essential as it determines how much energy is needed to break up an exciton into an electron and a hole, thereby creating free charge carriers. As such, a lower binding energy is preferable for solar cells or other optoelectronic devices [11]. The diffusion length can be defined by the distance that a carrier can travel before undergoing recombination. High diffusion lengths together with low exciton binding energy can enhance photoconductivity [12], which are optimal properties for devices like solar cells or phototransistors. However, electronic properties will always depend on the film deposited and how it crystalizes. This may lead to different band gap values and different band structure [13].

Another characteristic of MAPI is the possibility of ambipolar conductivity. This property is related to the doping character of the material and its electronic band structure. MAPI band structure allows for an electron effective mass similar to its hole effective mass. This balance between the effective masses, can originate the ambipolar conductivity seen in some MAPI films and MAPI devices [1]. However, this conductivity of n-type and p-type is not always the same, as it is derived from different causes and it is still uncertain what the origin is [14], [15]. One parameter that impacts the conductivity is the excess or deficiency of concentration of MAI and PbI_2 [6].

Ionic migration is a property present in perovskite materials. Through the application of an electric field, the ions and ionic defects will move and be redistributed. This property is a cause for concern on MAPI optoelectronic devices as it causes hysteresis, an enhanced material degradation and non-linearities that lead to changes in electrical characteristics. Ionic migration can also lead to reduction of charge carrier mobility and density. Due to these disadvantages, ionic migration keeps being studied so that it can be reduced allowing for the improvement the application of MAPI in optoelectronic devices.

1.2.3 Optical properties

The optical properties of MAPI vary depending on the deposition conditions [2]. Overall, the main optical properties of MAPI that attracted their use for optoelectronic devices were the high absorption coefficients (higher than the usual absorbers used in thin-film solar cells)[9], tunable and direct band gaps. Most of the optical properties have an interaction and depend on the electronic properties of the perovskite material. The optical absorption is one of such parameters as this is inherently related to the density of states and the electronic transitions between the CB and the VB [1]. This high optical absorption is also related to the long carrier diffusion lengths, which reduce the probability of a non-radiative recombination. Furthermore, MAPI perovskite is a direct band gap material which provides a better absorption when compared to previous solar cell absorber materials like crystalline Si.

1.2.4 MAPI transistors

Despite the advances on MAPI optoelectronic devices such as solar cells and LEDs, MAPI field-effect transistors have less reports and have not reached the applicability and performance or that other optoelectronic devices have [6]. Numerous reports manage to produce MAPI transistors with great properties but always with significant disadvantages that hinder the applicability of the FET [16]. Such problems can arise

from ion migration, one of the main causes of hysteresis, or from differences in polarization that come with temperature changes. As the temperature increases, poorer performances are observed [17]. As such, one of the key requirements for the applicability of MAPI FETs is stable operation at room temperature and higher temperature. Using different depositions methods and different solution configurations, like solvent ratios or the amount of precursor powders, it is possible to achieve devices with less hysteresis and with more thermal stability but still with mobilities inferior to the predicted [16]. These predictions are based on the reported low effective charge carrier mass. Through theoretical photoconductive studies the mobility of single crystal MAPI is measured to be between 500 to 800 cm^2 /Vs [6]. However, to this day, even optimized single crystal MAPI films achieve around 50 cm^2 /Vs [6].

There is still promise due to the inherent electrical properties of MAPI perovskite but there are main problems that need to be addressed in order to have reliable MAPI transistors. The aforementioned hysteresis has been intensely reported and studied [3], [6], [13], [16]. Using single crystal perovskite transistor or using solution-processed solution devices showed to lower the hysteresis in some studies, even though not eliminating it completely. Environment stability is also a recurrent problem in MAPI FET transistors as they are not stable enough at ambient conditions and can be degraded easily.

The characterization of the transistors is mainly done through the analysis of the transfer and output curves. The transfer curve gives parameters that allow for better understanding of the transistor performance.

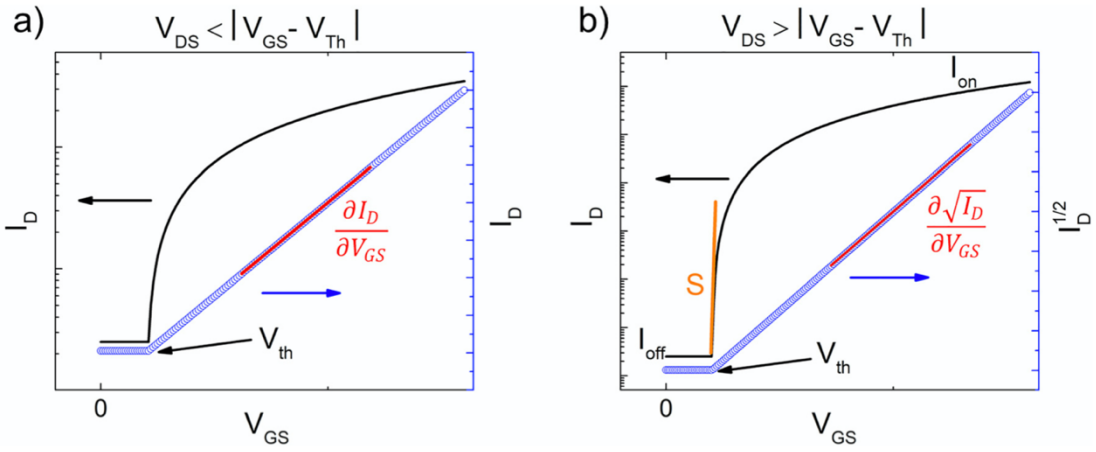

Figure 2 – Ideal behavior of a transistor transfer curve in linear (a) and saturation (b) regime.

The threshold voltage, V_{th}, is defined by the beginning of the current rise. Since this voltage determines when the device activates, if V_{th} is high, then the device is only operable at high voltage ranges, which is detrimental to most applications as it requires a high use of energy.

The subthreshold swing *(S)* is a figure of merit to measure how fast can the transistor switch on and off. S can be determined in the saturation regime through equation (1). In an ideal transistor, this parameter should be as low as possible. The lower this value is, the faster the switching between ON and OFF states can happen, indicating the device is appropriate for fast switching applications.

$$S = \frac{\partial V_{GS}}{\partial(log_{10}(I_D))}, \quad (1)$$

Another parameter related with the ON and OFF states is the I_{ON}/I_{OFF} ratio. This value should be as high as possible as it is the figure of merit to determine whether the transistor has a good distinction in its OFF and ON states.

In addition, both the linear and saturation mobilities can be determined through the transfer curves.

$$\mu_{lin} = \frac{L}{C_i * W * V_{DS}} * \frac{\partial I_D}{\partial V_{GS}}, \quad (2)$$

$$\mu_{sat} = \frac{2L}{C_i * W} * \left(\frac{\partial \sqrt{I_D}}{\partial V_{GS}}\right)^2, \quad (3)$$

In equations (2) and (3), W is the width of the electrodes, L is the distance between electrodes, C_i is the capacitance of the dielectric. These equations are only valid in their respective regimes.

MAPI transistors usually adopt the bottom gate/top contact architecture as it is the simplest configuration to fabricate. This architecture consists of the deposition of the dielectric on top of the gate, followed by the channel deposition and, lastly, the contacts.

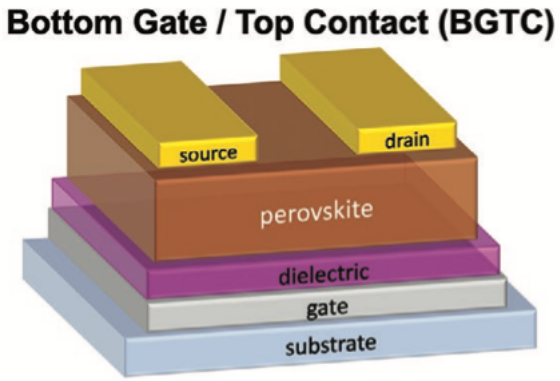

Figure 3 – Bottom Gate FET configuration employing the perovskite layer as channel.

Furthermore, while MAPI has great electrical properties, the rest of the transistor components also play an important role. This is mostly due to the interfaces of the perovskite with the dielectric and with the contacts. The roughness and reactivity of the dielectric needs to be studied as it might introduce defects and interfacial traps. SiO_2 is a commonly used material as a dielectric due to the ease of fabrication, the availability, and the low surface roughness. The contacts used for perovskite FETs are commonly Au. However, reports mention that gold can chemically react with perovskite. As such, new alternatives have been studied [6].

2

MATERIALS AND METHODS

This chapter covers the first phase of this thesis which consists of the experimental procedure for the deposition of MAPI films and the discussion of the studies done on each step of the procedures in order to understand how these steps influence the final film. For the studies done on the parameters' changes, it is important to note that not all were made in the same day and comparisons between films from different days might have some differences, even with the same conditions. Nevertheless, the final program for film deposition will be reproducible as it is one of the goals of this thesis but between studies some films will look different as they are not the final optimized film.

2.1 Description of the experimental Procedure

In this section, experimental procedure for the deposition of MAPI films will be explained in detail. This process consists of the solution preparation, the substrate preparation, and the film deposition via spin-coating.

2.1.1 Solution Preparation

For the solution of MAPI, PbI_2 and MAI precursor powders are put in a flask with the appropriate concentrations. The solvents (DMF-DMSO-GBL) are added posteriorly with the volume stipulated. After that, the solution is left stirring overnight in ambient conditions at 65 °C. The volume of solution can change according to the number of samples to be deposited. The volume of solvents and quantity of precursors added is changed accordingly as well, in a way that keeps the concentration and ratio the same. Different solutions with different solvents, solvent ratios, and precursor concentrations were experimented. These different solutions offered different results when deposited and those will be shown ahead.

2.1.2 Substrate Preparation

The material used as a substrate used was a 500 nm and 100 nm thick SiO_2 layer coated Si wafer. The wafers were cut in 2cm x 2cm substrates.

The substrates used were immersed in a beaker with acetone and placed 15 minutes in an ultrasound bath at 60°C. Posteriorly, they are rinsed with water and immersed in a goblet with water at the same temperature. Finally, after another rinse, they are put in IPA for more 15 minutes, rinsed with water and dried with a nitrogen gun.

Before deposition, the substrates are subjected to a 40 min Ozone UV treatment to remove the rest of the particles in the substrate, finalizing the cleaning. During this treatment they were also submitted to a temperature of 60 ºC.

Additionally, to understand and study the transmittance, reflectance and absorbance of the perovskite films, glass substrates were also prepared for deposition. These glass substrates, however, were cut into larger sizes: 2.5cm x 2.5cm. The cleaning of the glass substrates has some extra steps. Firstly, they are put in a goblet with water and 1% concentration of detergent (Hellmanex). Afterwards, they are put in the ultrasound bath for 30 min at 40 °C, rinsed with water twice. Another ultrasound bath in water may be applied if the substrates still show some remains of detergent. After these 2 steps, the same process as the Si/SiO_2 substrate cleaning is applied.

2.1.3 Film deposition via spin coating

The deposition process is a two-step spin coating deposition of a single MAPI layer. Prior to the deposition, the nitrogen gun is used on the substrates to remove any possible dust particles that adhered to the surface after removing the substrates from the ozone UV treatment. After that, the substrates are pre-heated in a hotplate at 80°C. The speed parameters were optimized to produce a better film, such details will be explained further ahead in this chapter. The deposition is composed of a first step of slower speed that lasts 10 seconds and of a faster second step that lasts for 20 seconds. During the second step, an anti-solvent is introduced (Chlorobenzene) in a quantity that is studied further ahead. Following the spin-coating, the sample is annealed on a hotplate at a temperature that was also studied and optimized.

2.1.4 Scanning Electron Microscopy

The SEM images were obtained using the Tabletop microscope TM3030 Plus Hitachi and the Hitachi Regulus SU8220.

2.1.5 Ultraviolet-Visible (UV-VIS) Spectroscopy

The UV-vis measurements were made using a Perkin Elmer Lambda 950.

2.1.6 Photoluminescence (PL) Spectroscopy

The photoluminescence data was obtained using the PerkinElmer LS 55. The measurements used a emission scan type with an excitation wavelength of 450 nm and a scan range from 500 nm to 900 nm.

2.1.7 X-Ray Diffraction (XRD)

The equipment used was the X-ray diffractometer (PANalytical Xpert PRO MRD). The source of the X-rays used was of Cu K-alpha with a wavelength of 1.540598 Å.

3

RESULTS AND DISCUSSION

3.1 Optimization of solution parameters

Perovskite solutions can be made using a variety of precursors and solvents with different concentrations [18]–[20]. In the case of MAPI, the concentration of the precursors MAI and PbI_2, the solvents ratio and type, can influence the deposition. In this section, these parameters were tested in different solutions with the intention of selecting a solution to investigate the remaining parameters.

3.1.1 MAPI Precursors

Two configurations of precursors were explored in this study: a MAPI-1 variant and a MAPI-2 variant. The precursor concentrations are listed in Table 1, and the solutions can be seen in Figure 4.

Table 1 – Precursors concentration for MAPI solutions.

MAPI-1		MAPI-2	
PbI_2	**MAI**	**PbI_2**	**MAI**
0.3 M	0.5 M	1 M	1 M

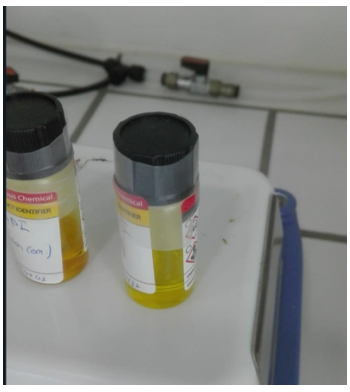

Figure 4 – MAPI solutions in the hotplate.

From the SEM images (Figure 5) it is very clear that there is a difference when comparing the films both variants. Under the same conditions, the MAPI-2 shows better coverage and crystallinity. This does not necessarily mean that the MAPI-1 is not valid to deposit thin films, but that the conditions for it must be

better optimized. Since the impact of the various steps in deposition are being analyzed, the use of the MA-PI-2 solution was chosen as to ensure the deposition of a good and reproducible MAPI film.

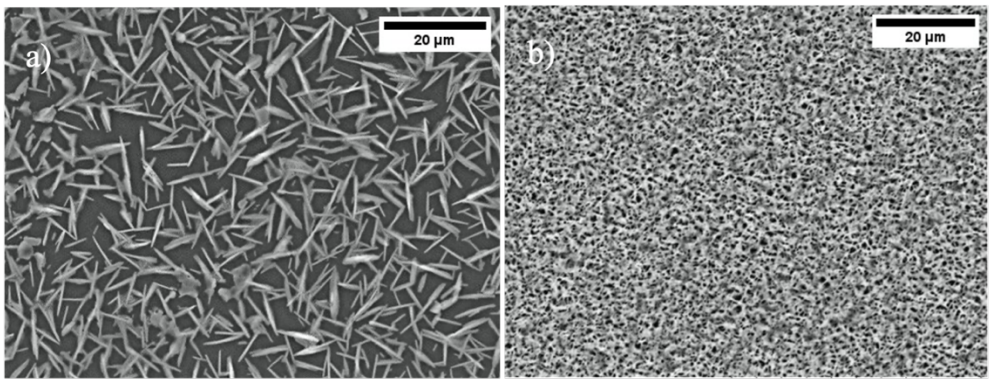

Figure 5 – SEM images for MAPI-1 (a) and MAPI-2 (b).

3.1.2 Solution Solvents

The solvents tested for the solution were three: DMF, DMSO and GBL. The combinations were DMF+DMSO (8:2 ratio), and DMSO+GBL (7:3 ratio). Both these combinations were tested to see which was the solution that could form films with better coverage. Both these films were deposited with the same spin-parameters and an annealing at 100 °C for 10 minutes in a dessecator annealing (annealing studies described further ahead).

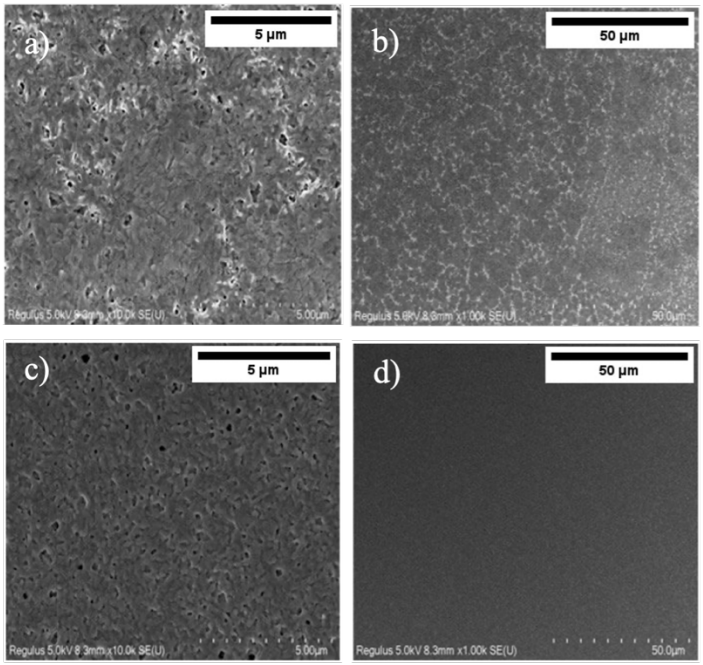

Figure 6 – SEM images for GBL+DMSO MAPI: 10k (a) and 1k (b) and DMF+DMSO MAPI 10k (c) and 1k (d).

Both MAPI solution configurations show films with a good coverage and a few numbers of pinholes. There is, however, a difference in the crystallization of the films. In Figure 6 it is possible to see that the films from the solution of GBL+DMSO have bright spots across the entire film. These can be due to different crystallization phases due to the charging of non-conductive material that interacted with the electrons from the SEM in different ways, generating the contrast between both solutions. Another possibility for these

bright spots is the existence of trapped solvent. This can be due to the fact that both DMSO and GBL have high boiling points and the annealing was not sufficient to evaporate the solvent.

Due to the more homogeneous crystallization and good coverage that DMF+DMSO solution films present (Figure 6 c) and d)), this solution was chosen to be optimized for the subsequent deposition studies.

3.2 Optimization of substrate preparation

3.2.1 Ozone treatment

The ozone UV step [21], as a last step of the cleaning procedure, is essential as, without it, the MAPI solution does not adhere sufficiently to the surface of the substrate and leads to films with very poor coverage. The time of ozone UV exposure was investigated as to find the optimum for the film formation.

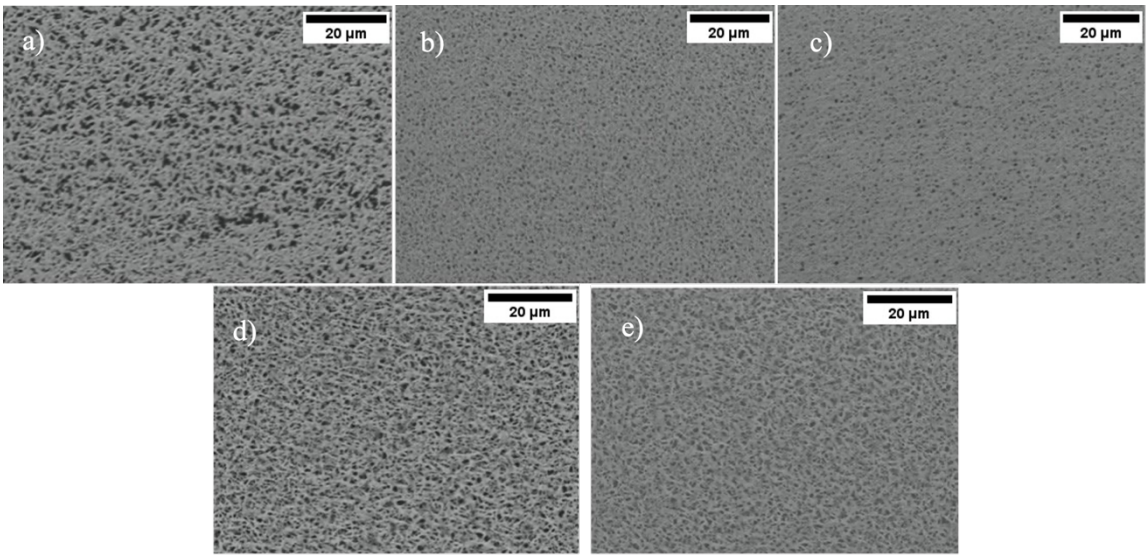

Figure 7 – SEM images of the impact of ozone exposure in Si/SiO_2 during 20 (a), 30 (b), 40 (c), 60 (d) and 85 (e) min.

As it is possible to see in Figure 7, the ozone exposure shows to be an important parameter when it comes to film coverage. When the exposure is inferior to 30 min, the MAPI film still has difficulty in forming, probably due to the time not being enough for the full cleaning of the SiO_2 surface. After 30 and 40 min of ozone treatment, the films show better coverage. There is still a considerable quantity of pinholes in these samples, however this is a preliminary study where the rest of the parameters have not yet been optimized. When the exposure goes over 40 min, the films start showing less coverage again with the existence of an increased number of pinholes. This might be because over-exposure to UV ozone treatment can degrade the SiO_2 surface [22]. This shows that the ozone exposure needs to be within the 30 and 40 minutes to ensure that the films have the best coverage. The less pinholes the film have, the better optoelectronic properties like lateral conduction and absorption [23].

Nevertheless, ozone UV time of exposure is not enough to have a pinhole-free film and the spin coating deposition needs to be studied to understand how such films can be produced with ease of reproducibility.

3.3 Optimization of spin-coating deposition

3.3.1 Spin Parameters

The spin rate of deposition has a strong impact on the final film. This is especially true for the second step. This step is crucial because it is the part that the anti-solvent is introduced to start the evaporation of the solvent and, as such enhance the crystallization of the perovskite. As such, the speed of this step will influence how the anti-solvent is spread in the perovskite film. For the speed studies, all the other parameters, like the annealing temperature or the volume of anti-solvent dropped were maintained the same. The substrate for these studies was SiO_2.

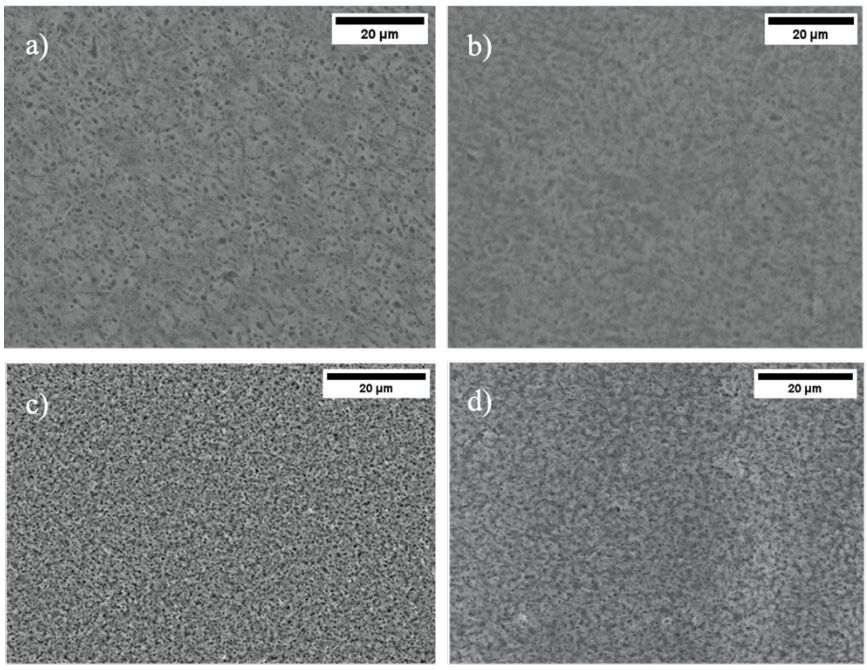

Figure 8 – SEM images of MAPI films at different 2nd step speeds (a - 3000, b - 4000, c - 5000, d – 6000).

From all the studies it could be gathered that the faster the second step, the better the deposition. This suggests that in addition to the anti-solvent enhancing the crystallization of the film, an increase in spin rate can have a similar effect. This needs to be moderate as a faster speed can mean that some solution is expelled from the substrate. From the observing Figure 8, 6000 rpm for the second step speed offered better deposition with better crystallization and coverage.

3.3.2 Anti-solvent washing

3.3.2.1 Anti-solvent

There are multiple antisolvents that are used to help the crystallization of perovskite [24],[25]. In this study, two anti-solvents were tested: chlorobenzene and toluene. The test was made using the same spin-coater program and annealing conditions, changing only the anti-solvent. The results were evident to the naked eye even before analyzing the samples with the SEM. The toluene-washed films showed poor coverage of the substrate and were opaquer and dirtier. The difference in the film crystallization can be seen in Figure 9. This led to the decision of using chlorobenzene as the anti-solvent to be optimized.

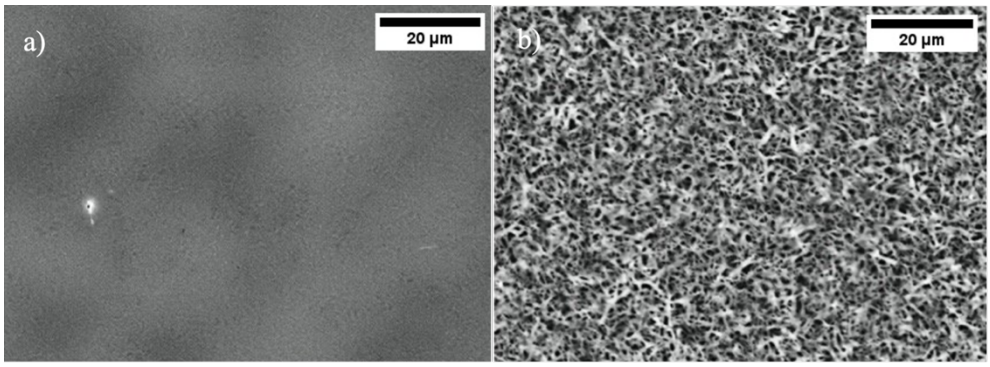

Figure 9 – SEM images of Chlorobenzene (a) and toluene (b) washed MAPI films on glass.

3.3.2.2 Method of anti-solvent washing

The more common method of anti-solvent washing is the introduction of the anti-solvent during the spin-coating. However, there are other techniques that can help the crystallization of the perovskite. One of these techniques would be the dipping of the film post deposition and right before annealing [26]. A container was filled with the anti-solvent and then the film was immersed in that container until de film started to change to brown color or just for 2 seconds.

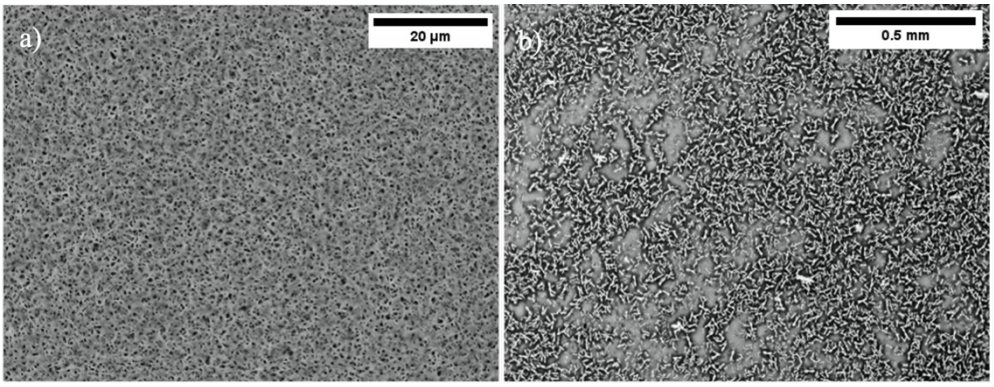

Figure 10 – SEM images of MAPI films with Antisolvent dropping method (a) and antisolvent bath method (b).

This technique did not show any improvements as both the time of dipping for 2 seconds and the type of anti-solvent used, produced films with worse coverage and crystallization as can be seen in Figure 10. Furthermore, this method of anti-solvent washing is not practical as it requires the insertion and removal of a thin sample in small container. This needs a constant renewal of the anti-solvent for every film and is very wasteful. Additionally, the less antisolvent is used in the container, the harder it is to submerge the film completely. When these observations are added to the poor results this technique brought, it can be concluded that the anti-solvent drop during the spin-coating is better for the deposition of MAPI films.

However, the second step lasts for 20 s and so it remains to be studied whether the time of dropping the anti-solvent has any impact on the final film. Most of the films deposited prior to this study were anti-washed 5 s into the second step. A comparison (Table 2) was made to see if the time of dropping the anti-solvent would affect the film coverage.

Table 2 – SEM images of MAPI films with different anti-solvent dropping times.

0 s	5 s	10 s
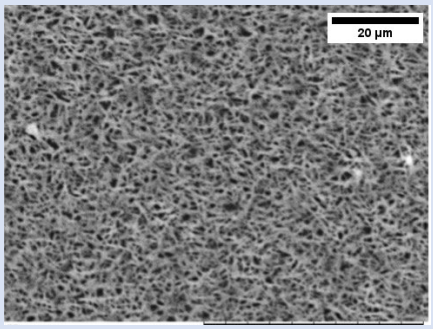	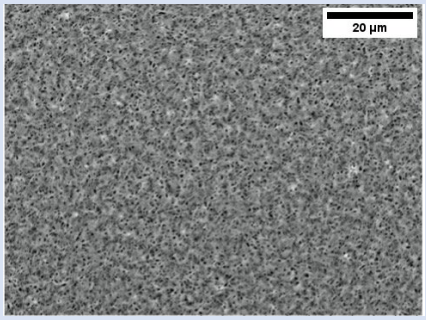	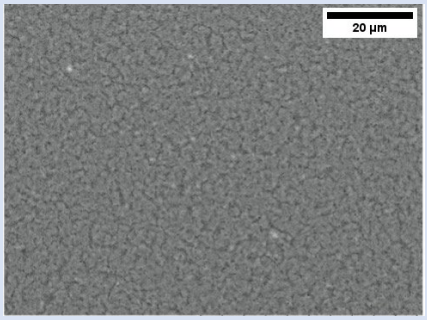

Overall, dropping the anti-solvent 10 s into the 2nd step reveals to be a better method than dropping it earlier. Besides the better coverage and reduced number of pinholes that can be seen in the SEM, the films adopt a more clear, shiny color. This color is more similar the color achieved when depositing the MAPI films inside the glove box, even though it is still not as black as the glove box films. With these results, the 10 s dropping was chosen as the optimal one for the antisolvent dropping.

3.3.2.3 Dropping of anti-solvent

The anti-solvent dropped during the spin-coating is another parameter that impacts the quality of the film. If the perovskite film is not submitted to the effect of anti-solvent washing, not only will the perovskite not crystalize but it will also have very poor coverage and, in some cases, will not adhere to the substrate.

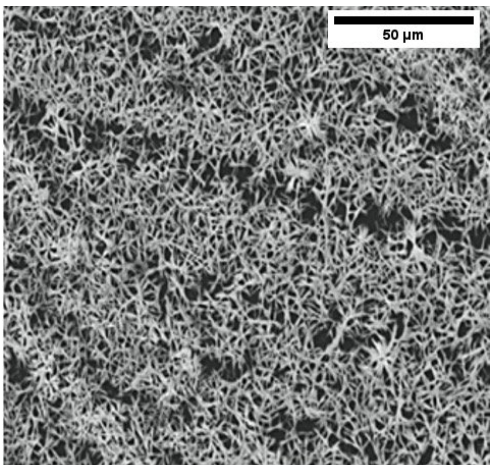

Figure 11 – SEM images of a MAPI film without antisolvent washing.

Until this test, 60 µL of antisolvent was being used for the film's deposition, and so, the volume was increased to compare the different films. Figure 12 compares the different volumes used.

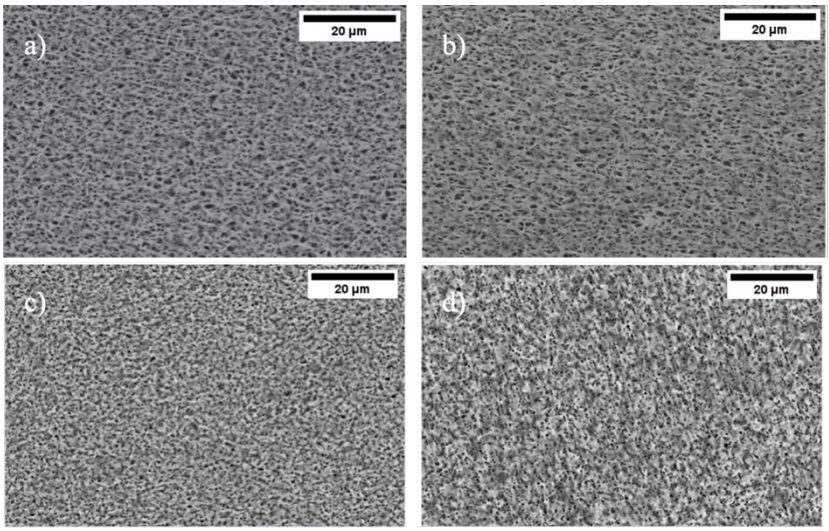

Figure 12 – SEM images of MAPI films with different volume of anti-solvent dropped (a-80 µL, b-100 µl, c-150 µl, d-200 µL).

The clearest difference is the reduction of pinholes from the film. From 100 µL to 150 µL there is a difference in the crystallization of the film, a better crystallization to form although with a considerable number of pinholes, but with total coverage. With lower volume than 100 µL the crystallization is very poor with not just pinholes but incomplete surface coverage. The increase in volume of the anti-solvent shows an increase in coverage and reduction of the number of pinholes. This relation remains true for other configurations of depositions conditions. However, while 200 µL of anti-solvent achieves the best results, after all the relations and studies have been made, there is no need to use such an amount, and 125 µL of chlorobenzene was enough. This relates to the findings of the best solution volume, the optimized spin-coater spin rate, and the optimized annealing. If a film can be achieved with less chlorobenzene, then it should be done. Nevertheless, an excess amount of chlorobenzene as anti-solvent does not show any apparent damage on the film.

Furthermore, the height from which the antisolvent is dropped can heavily influence the film quality. If the antisolvent is too close or afar from the film, a circular defect (Figure 13) appears in the surface of the film.

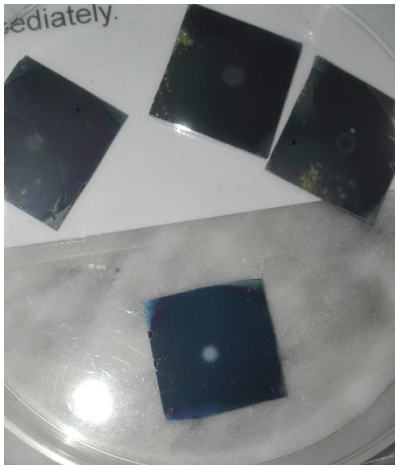

Figure 13 – Photograph of MAPI films with circular defects.

These circular defects prevent the crystallization of the perovskite across the entire film but specially in the center. This can be confirmed though Figure 14. In these films, there is the existence of white stripe

structures that cover the center of the film. As the film starts nearing its borders, these structures start to be less common but still cover a great part of the film (Figure 14), making the device fabrication with these films not optimal.

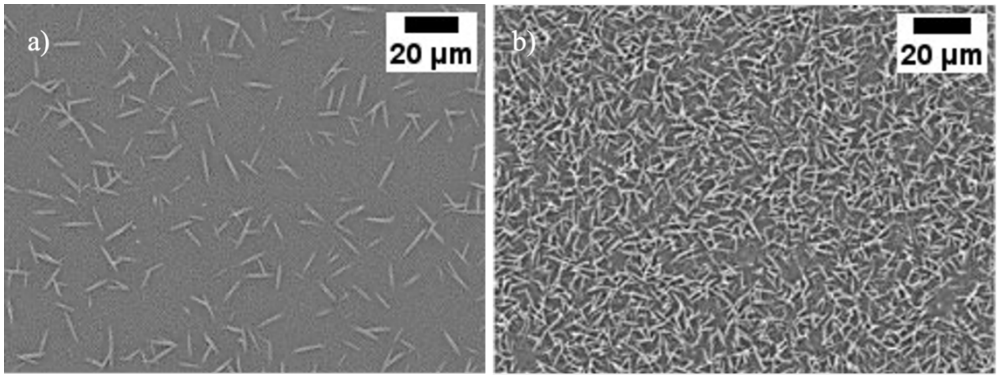

Figure 14 – SEM images of MAPI films with circular defects: corner (a); center (b).

3.4 Optimization of film annealing

3.4.1 Method of annealing

The annealing step takes place right after the spin-coating deposition and is crucial for the production of pinhole free films. There are various types of annealing that can be done but the most common one is on a hotplate. As the annealing is made under ambient atmosphere conditions the influence of oxygen and humidity for the deposition of the films affects not only the spin-coating deposition, but also the annealing [27].

Because of those reasons, various methods of annealing were tried in this thesis, so that the disadvantages of deposition in ambient conditions can be compensated. For all these methods the annealing conditions were 100°C for 15 min.

One of such techniques was a solvent annealing method. This technique was an adaptation of the method developed by *Ge et al* [28]. Using a glass petri box, 5 drops of 20 µL of DMF were dropped. After the spin-coating, the film as placed in the petri box where the annealing is done. This method is not very practical in these conditions as when the petri box heats, some drops condensate on its ceiling and can fall on the film, damaging it, which led to the decision of not using this as the final method. The film annealed with this method (Figure 15) showed the formation of some streak like structures along with the grains which can be related with the bad crystallization of the perovskite material. Additionally, the white spots on the films can be attributed to PbI_2 formation, further showing the lack of perovskite crystals.

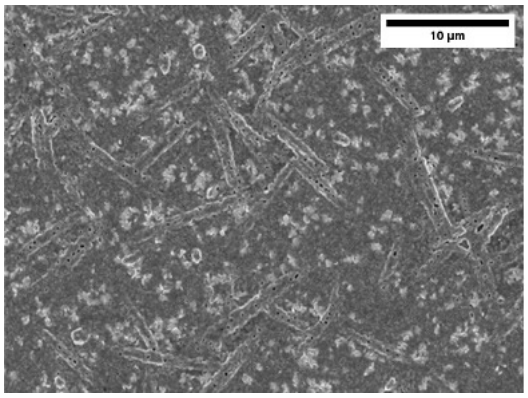

Figure 15 – SEM image of a MAPI solvent annealed film.

Another method tested was the vacuum annealing [29]. This consists of doing the common hotplate annealing but in a vacuum desiccator. The vacuum annealed films showed very few pinholes and in a range that does not interfere with the 50 µm channel lengths for future transistor deposition. Additionally, the regular hotplate annealing showed an increased number of pinholes when compared with the vacuum annealing (Figure 16).

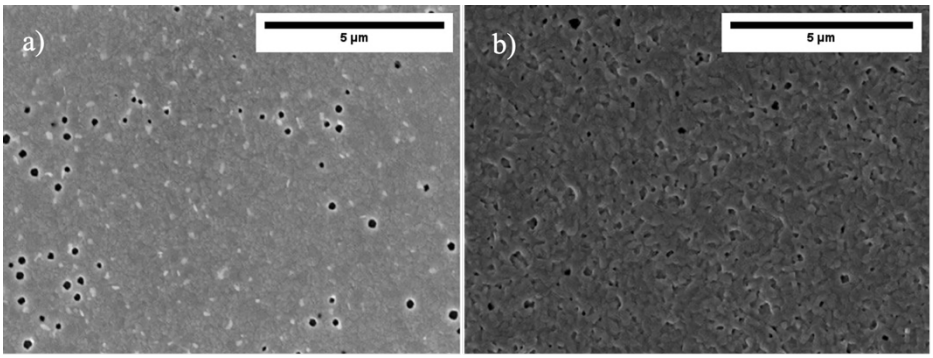

Figure 16 – SEM images of hotplate annealing (a) and vacuum annealing (b).

An additional annealing technique that has achieved successful results was the two-step annealing [30]. After the film is put through a hotplate annealing at a lower temperature, it is then put in a hotplate at a higher temperature. This second step can be done immediately after the first annealing or after an hour rest. Since the results with the desiccator were positive, it was also tried using a vacuum annealing for the second step. This vacuum annealing second step was also done after one hour rest. The results can be seen in Figure 17.

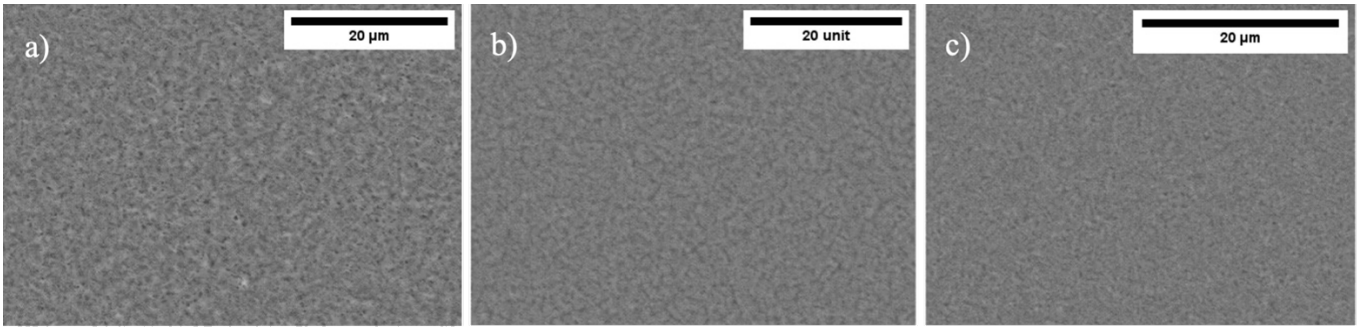

Figure 17 – SEM images of 2-step annealed. MAPI films: 1 hour rest (a), desiccator (b), immediately after (c).

The results of this study were positive as the films show either no pinholes, or a low quantity with short diameter. There is no need to leave the samples resting one hour since the films annealed without rest

have better coverage and less pinholes. Both the desiccator 2-step annealing and the 2-step hotplate with no rest allowed the formation of films with coverage of the entire substrate and with no pinholes.

3.4.2 Annealing Temperature and time

Even though pinhole-free MAPI films with good coverage were achieved through the vacuum desiccator annealing and the 2-step annealing, the goal of this first phase is to optimize MAPI deposition with as much simplicity as possible. As such, the regular one-step one place annealing can be further optimized.

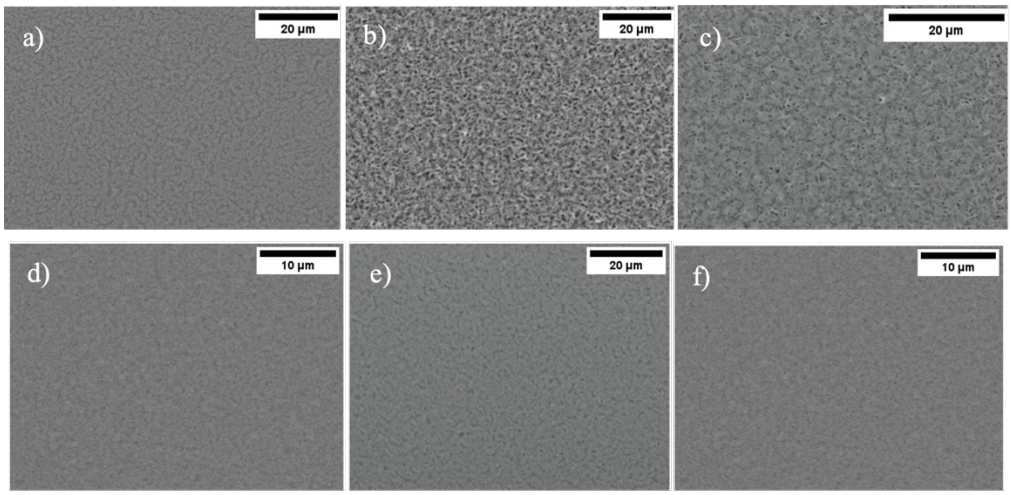

Figure 18 – MAPI films with different annealing temperatures: 90°C for 15 min (a) 100°C for 15 min (b) 110°C for 15 min (c); 90°C for 30 min (d);100°C for 10 min (e); 110°C for 5 min (f).

One of the main takeaways from these annealing investigations is the effect of over annealing and under annealing. A balance needs to be achieved between the time of annealing and the temperature. As is possible to see in Figure 18 a), when the temperature is 90 °C, 15 minutes is not enough for the formation of the perovskite film in the entire substrate. This can be seen by the presence of perovskite island structure with spaces between them meaning that the perovskite hasn't fully covered the film and the crystallization is not complete. This will hinder the lateral conduction of the films

On the other hand, if the film is exposed to annealing for more than necessary, there starts to be the formation of pinholes, which also decreases the lateral conduction of the film. This is confirmed in Figure 18 as the change in annealing configuration from 90 ºC for 15 minutes to 30 minutes reveals a better coverage and the lack of these island structures. As for the temperatures of 100 ºC and 110 °C, by reducing the time of exposure to temperature, the number of pinholes reduced, and the films show overall better coverage. Through the photoluminescence analysis, further information with respect to the different annealing can be gathered. This information can be obtained using the full width half maximum (FWHM) of the PL data (Figure 19). This parameter is defined by the width of the line shape at half of its maximum amplitude. Comparing the FWHM allows to compare the structure of the films. A lower FWHM corresponds to better crystallinity. The FWHM of the different annealed films can be seen in Table 3.

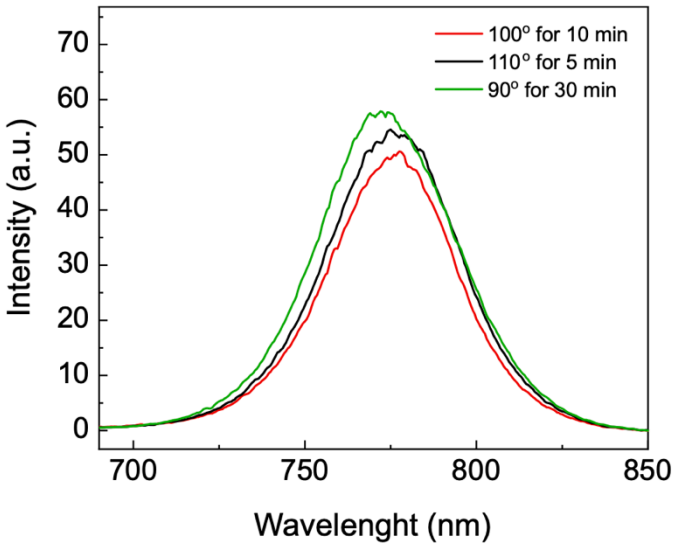

Figure 19 – PL spectra of MAPI films with different annealing temperatures and times.

Table 3 – FWHM (nm) of MAPI films with different annealing temperatures and times.

90ºC for 30 min	100ºC for 10 min	110ºC for 5 min
47.92 nm	43.94 nm	45.58 nm

While the difference is nanometers is not big, since the SEM images are similar this parameter will be used to choose the better annealing time and temperature. It is important to note, however, that a 2 nm difference is within error margins.

These results indicate that annealing the MAPI films at 100ºC for 10 minutes achieves a film with slightly better crystallinity than the other annealing configurations.

3.5 Volume of solution applied on the substrate

The last study to be made was to understand whether the volume of solution dropped onto the substrate before spin-coating impacted the deposition. This study was done because the spinner gets dirty once the first step starts. This means that some perovskite solution is being expelled from the substrate due to fast rotation of the process. Nevertheless, since the speed studies were done, reducing the speed would act against the optimization. Therefore, more solution was used to compensate the solution that leaves the substrate during the procedure.

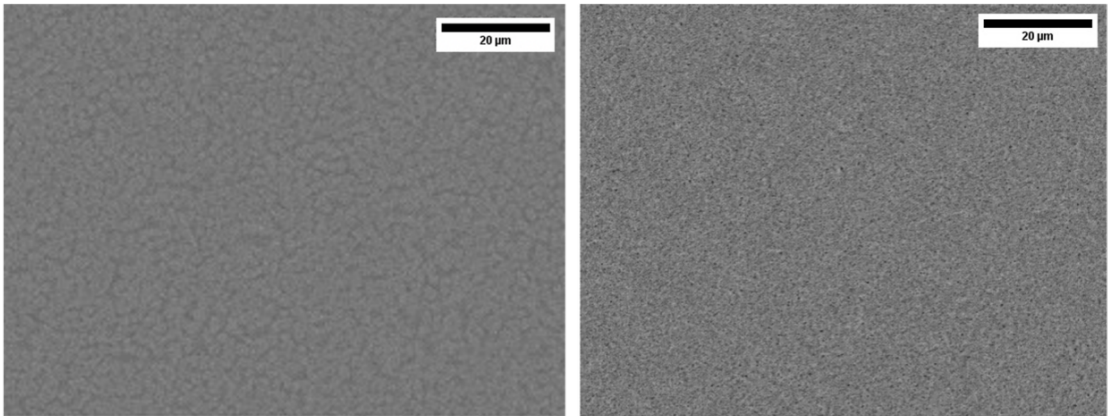

Figure 20 – SEM images of MAPI films: 80 µL of MAPI solution (a) vs 125 µL of MAPI solution (b).

One of the more changes on the films is optically. The films with 125 µL solution adopt a black, clear color, similar to the MAPI films deposited on a glovebox. This might have to do with the thickness of the films. The substrate of Si/SiO_2 has a clear dark blue color, and as such, less solution will make a thinner film that allows more light to pass through and interact with the substrate, leading to a film that does not appear to be back.

Analyzing the SEM imagens in Figure 20, with more solution, there is a full coverage more consistently. While using 80 µL also allowed such results in previous studies, the difference in color and the reproducibility are better in the 125 µL samples. When using 80 µL, some films will show no pinholes, but some spots in the film that are not well covered. This phenomenon can be seen in some pathways that appear in the SEM image, where it looks more like an aggregate of perovskite structures, and not an uninterrupted film.

3.6 Film Properties

The final deposition conditions for the film can be seen in Table 4.

Table 4 – Final configuration for MAPI film deposition.

Ozone Time	40 min
Solution Solvents ratio	DMF and DMSO (9:1)
Volume of solution dropped	125 µL
1st step speed	2000 rpm
2nd step speed	6000 rpm
Acceleration of 2nd step	5000 rpm/s
Anti-solvent	Chlorobenzene
Volume of antisolvent dropped	125 µL
Annealing Method	Hotplate annealing
Time and temperature of annealing	100°C for 10 min

To characterize this material optically, the UV-VIS spectroscopy, photoluminescence spectroscopy and XRD techniques were used.

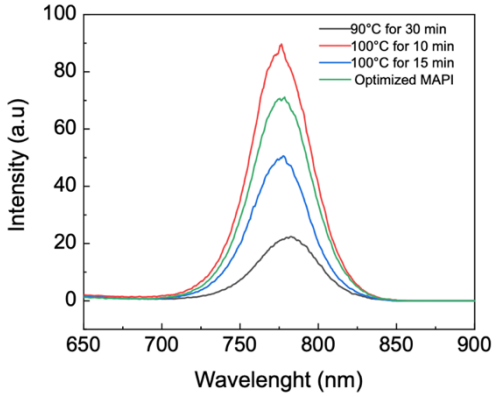

Figure 21 – PL spectra of optimized MAPI and previous MAPI films.

Table 5 – Annealing conditions of different MAPI films.

Gg23	Gg25	Gg15	Optimized MAPI
90°C for 30 min	100°C for 10 min	100ºC for 15 min	100°C for 10 min

From the photoluminescence measurements (Figure 21) it's possible to see that the band gap of the semiconductor is at the 776.5 nm (1.59 eV).

The data, taken at room temperature, points to a low concentration of defects in the film, as there is only one peak of intensity and if some radiative defects were formed, other peaks with lower intensity would appear on the spectra. However, these defects might just have a low intensity peak that can only be seen at lower temperatures [31] so it is not possible to say with certainty that such is the case. Other films (conditions seen in Table 5) have the same band gap except for sample Gg23. The difference is that this film is annealed at 90°C. All the FWHM have very similar values that can be due to measurement errors of the equipment. Nevertheless, these errors are within 2 nm and do not change the conclusion from these results. The similar FWHM values are an indication that all samples have a similar crystal quality. While the intensity peak of sample Gg25 is higher than the optimized film, there is a clear difference in the coverage of the films as can be seen in Figure 22. These SEM imagens show that sample Gg25 does not have the film coverage to allow lateral conduction required for the transistor operation.

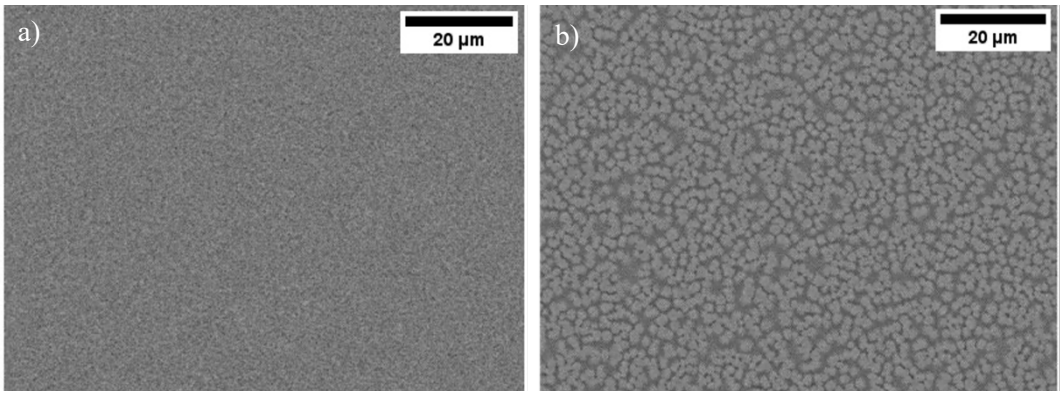

Figure 22 – SEM images of optimized MAPI (a) and sample GG25 (b).

Table 6 – FWHM (nm) of MAPI films.

Gg23	Gg25	Gg15	Optimized MAPI
45.69	45.73	44.35	46.22

These results are in favor of the optimization done as it shows that there as an improvement in the film coverage while retaining crystal quality. Another method to calculate the band gap of the material is through cutoff wavelength from the sample's absorbance spectra. The absorbance spectra can be determined through the UV-vis spectroscopy analysis seen in Figure 23. Due to the Si/SiO_2 substrate not being transparent and, as such, incompatible with UV-vis spectroscopy, a MAPI film deposited on a glass substrate was used for these measurements.

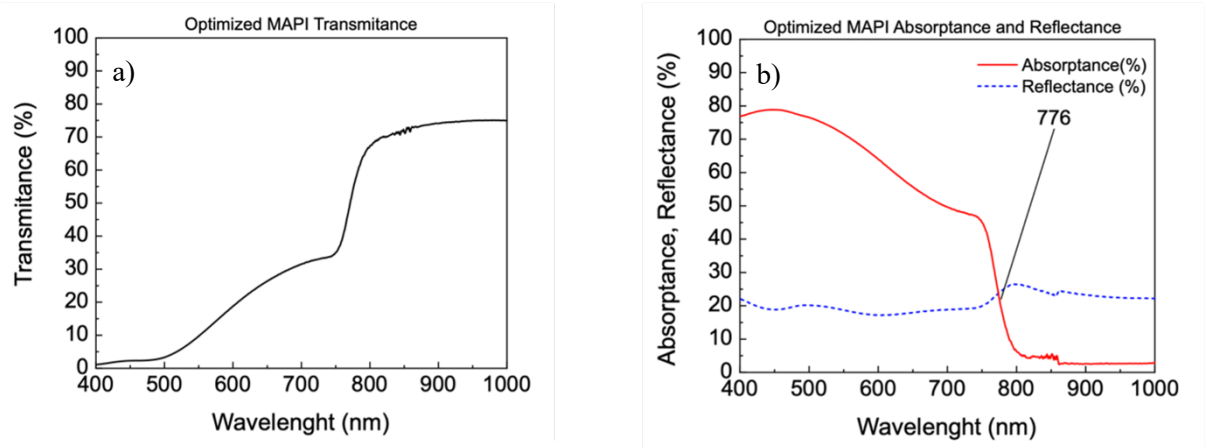

Figure 23 – Transmittance (a), Absorptance and Reflectance (b) spectra of optimized MAPI films.

The substrates for these samples are not SiO_2 but glass instead. The reason for the substrate change is because the UV-vis technique only works on transparent substrates.

Through the absorptance spectra, a Tauc plot (Figure 24) was traced in order to calculate the energy band gap. The band gap obtained was 1.604 eV which shows a difference when compared to the band gap determined through the photoluminescence. This slight shift in band gap value is likely due to the existence of the Stokes shift, which represents a difference in the band maxima of absorption and emission spectra of the same electronic transition [32].

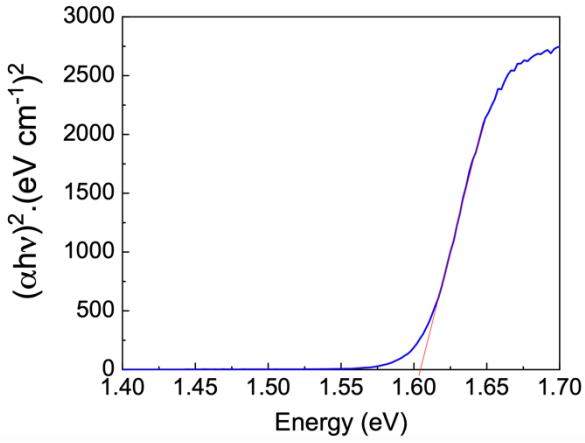

Figure 24 – Tauc plot and band gap determination of the optimized MAPI films.

Additionally, it can be inferred that little to no formation of PbI_2 happened since there is no absorption peak in the 536 nm of the absorptance spectra (Figure 23) which corresponds to 2.31 eV, the band gap of PbI_2.

In the XRD measurements (Figure 25), the excitation wavelength was 450 nm. The peaks of 14.09º, 28.42º, 31.83º, and 43.16º can be matched with the crystallinity tetragonal structure of perovskite, respectively, the (110), (220), (310) and (330) diffraction peaks [20], [33]. There is also a diffraction peak at 12.62º which can be assigned to the (001) peak of PbI_2. This means that there was not a total conversion of the precursor into perovskite. However, the low intensity of the peak coupled with the fact that there was no absorption peak for the PbI_2 in the absorbance spectra, suggests that the PbI_2 formation is not significant enough to affect the perovskite film properties.

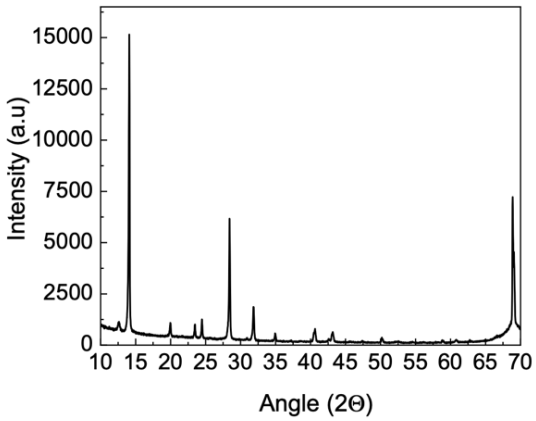

Figure 25 – XRD spectra of the optimized MAPI film.

3.7 Device Fabrication

For the device fabrication, there is only the need for the contact deposition. The wafers used already have a conductive gate, the Si, and an oxide, the SiO_2. The perovskite acts as the conductor. As such, there is only the need to deposit the contacts on top of the MAPI film. So, the devices fabricated were all bottom-gate transistors.

3.7.1 Contact deposition – Metal evaporation

The gold deposition was achieved through electron-beam evaporation on the SiO_2. Transistor masks with 50 um of channel length were placed in the transistor before the samples were put under vacuum at around 10^{-5} mbar of pressure. The vacuum reduces the particles in the chamber so that the focused electron beam impacts in the gold without any impacts, and so that the gold can be deposited with the maximum purity possible. The deposition starts with an electron beam generated with lower current so that the impact of the gold particles on the perovskite film does not degrade it. After the film has around 10 nm of thickness, the current is increased, and the deposition continues until there is an 80 to 100 nm layer of gold film.

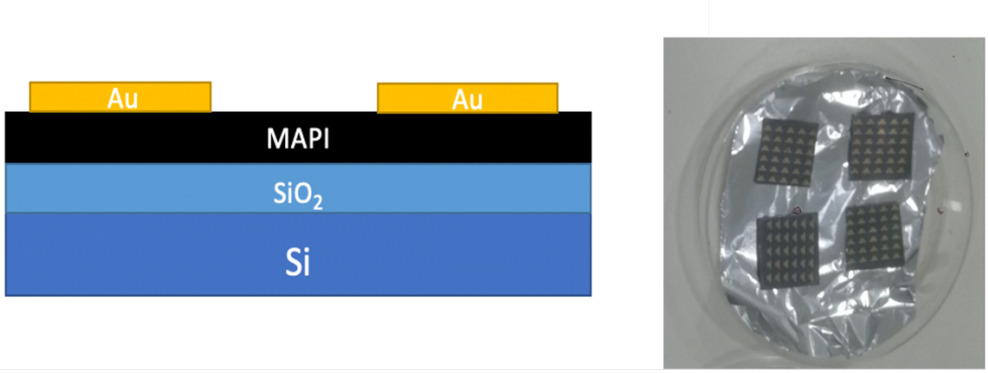

Figure 26 – Cross section scheme of the MAPI transistors and photograph of the MAPI transistors.

3.8 Device Characterization

3.8.1 Electrical characterization

There were two main temperatures at which the transistors were measured: at room temperature and at 200K, under vacuum. The interpretation of the transistor characterization and behavior is done through the analysis of the output and transfer curve. The output curve is traced by measuring the gate current values while the drain voltage increases. During these measurements, the gate voltage applied is constant. The transfer curve is traced measuring the drain current values as the gate voltage changes, keeping the drain voltage constant.

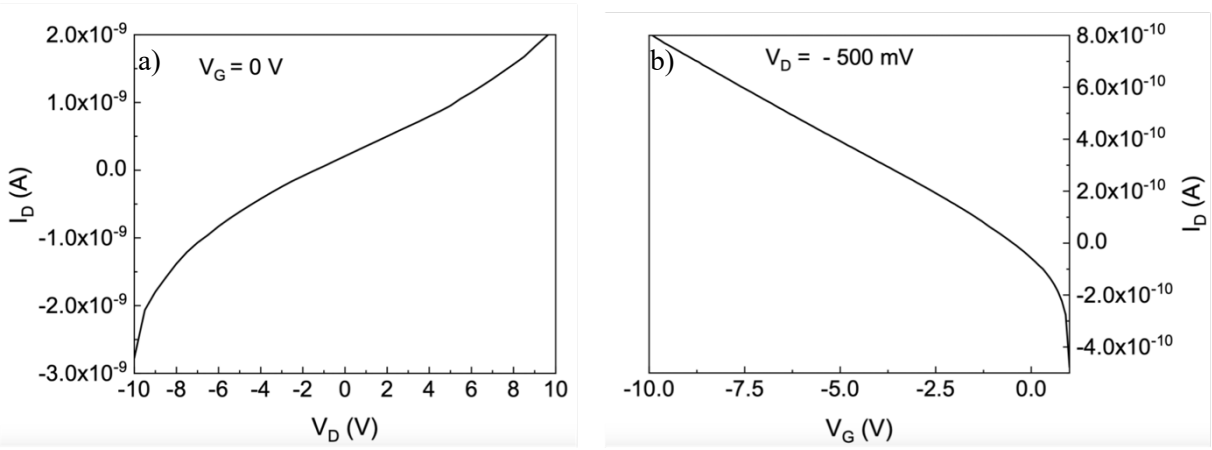

Figure 27 – Optimized MAPI transistor Output curve (a) and Transfer curve (b) at room temperature.

The output and transfer curve measurements (Figure 27) were measured under ambient conditions. The output curve obtained had a gate polarization of 0 V in order to ascertain the conduction of the perovskite material without gate modulation. Both the gate and drain currents are in the nA range which is low when compared with other MAPI transistor devices of similar geometries. This low current may be due to lattice defects that reduce the mobility and cannot be observed with SEM image. Another possibility is a reduced mobility due to charge carrier trapping at the SiO_2 surface. The output behavior has some non-linearities present as compared to the ideal curves seen in Figure 2. Nevertheless, the transfer curve presents a linear portion where the extraction of the characteristic parameters can be made as it is in accordance with the model presented (introduced in Section 1.2.4).

In these measurements, our devices did not reach the saturation regime. Furthermore, the perovskite material exhibits a p-type behavior under room-temperature and ambient atmosphere conditions.

Not every parameter can be extracted as the OFF region of the curve could not be measured. This means that during the transfer curve measurements, the devices were never in an OFF state. This can be potentially due to the hysteresis typically present in perovskite devices. Whether there is a forward scan or a reverse scan, the hysteresis effect will cause charge accumulation which might lead to the device never reaching an OFF state during the measurements.

Through this transfer curve, it is possible to extract the field-effect mobility of the device which had a value of $1.5 \cdot 10^{-6}$ $cm^2/V.s$. The saturation mobility cannot be extracted as the gate voltage is only 500 mV and with that voltage the device does not enter the saturation regime. Higher gate voltages cause an increase in both currents noise which leads to device instability, not being adequate for the extraction of the mobility.

To expand our analysis, the transistors, were measured at lower temperatures under vacuum, using a Janis cryogenic probe station. These results proved to be much better with drain currents in the range of uA. The output and transfer curves can be seen in Figure 28.

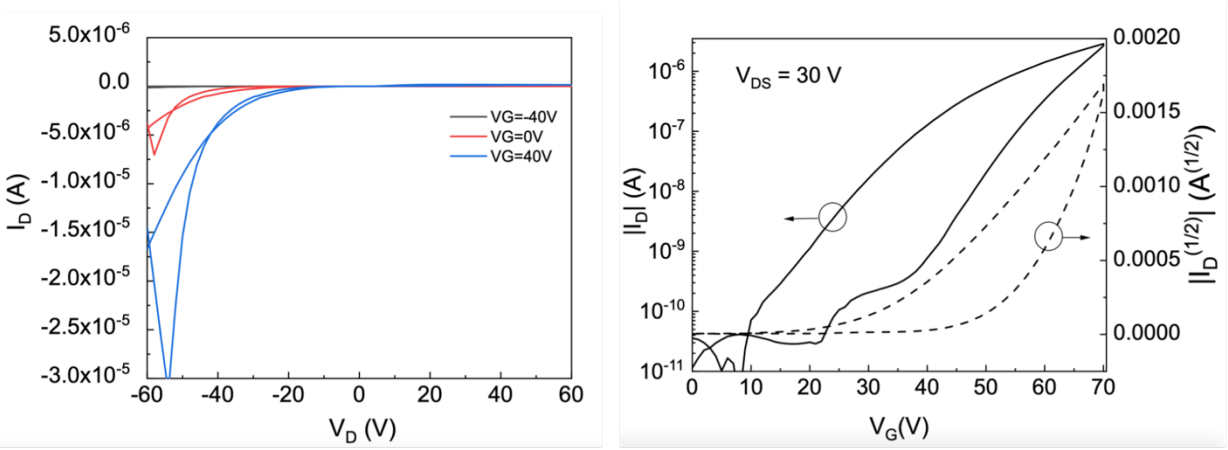

Figure 28 – Output and Transfer curves of MAPI transistors at 200K.

The devices exhibit a n-type behavior with an increase in the majority carriers (electrons) as the gate voltage increases positively. This is in contrast with the p-type behavior observed at room temperature. This is not unexpected as these materials are usually ambipolar with different conductivities in both types. By changing the temperature and surrounding atmosphere, the perovskite will have different electric properties, and so, a difference in polarity is within the expected. In addition, it is possible to see the gate modulation and the effect it has on the output curve.

The transfer curve has an exponential growth in the drain current. There is a high increase in the conduction of the transistor when the drain voltage gets lower. A problem with these devices is the clear existence of hysteresis that might be product of charge accumulation caused by charge trapping in defects or ionic migration [34]. With this in mind, it is known that ion migration is reduced at low temperatures due to the freezing of ions [35] and so, this hysteresis can be attributed to eventual defects that cannot be detected through the spectroscopy methods used. There are still some non-linearities in the transfer curve that can affect the proper and correct interpretation, as such, the extracted mobilities might be over/underestimated. To try to compensate this problem, the mobilities using the forward and reverse scan were used to have an interval of the potential mobilities in these devices with strong hysteresis.

Table 7 – Forward Scan MAPI transistor measurements at 200K

Ion/Ioff	Vth (V)	Ci (F/m^2)	S (V^{-1} dec)	μ_{sat} ($cm^2/V.s$)	μ_{lin} ($cm^2/V.s$)
10^6	35	$8.63 \cdot 10^{-1}$	8.54	$5.38 \cdot 10^{-5}$	$6.1 \cdot 10^{-5}$

Table 8 – Reverse scan MAPI transistor measurements at 200K

Ion/Ioff	Vth (V)	Ci (F/m^2)	S (V^{-1} dec)	μ_{sat} ($cm^2/V.s$)	μ_{lin} ($cm^2/V.s$)
10^6	56	$8.63 \cdot 10^{-1}$	7.04	$3.39 \cdot 10^{-4}$	$1.53 \cdot 10^{-4}$

Even though the mobilities values obtain can be considered low when compared to more recent MAPI transistors [6], these device measurements allowed for the electrical characterization of the perovskite film deposited, fulfilling the goal of this study.

In addition, recent transistors studies achieved better results at room temperatures which is a clear difference from the low temperature measurements in this study. One of the characteristics that can be inferred from the mobilities is the potential absence of contact resistance. Contact resistance affects the linear mobility in a stronger way than the saturation mobility, and as such, this is reflected on a much lower linear mobility. However, the values of both mobilities are of the same order, with similar values from which is possible to infer that there is not contact resistance. This is a positive quality as it means the gold deposited well on the perovskite without creating damage that might increase resistance. On the other hand, it also reflects that the low values can be attributed to a film problem and not in the device fabrication [47].

4

CONCLUSIONS AND FUTURE PERSPECTIVES

This work had the main goal of optimizing the deposition of MAPI on SiO_2 under ambient conditions. This work also focused on the electrical characterization of the MAPI perovskite material used in a transistor device. Considering perovskite materials are usually deposited under controlled conditions using a glovebox, the optimization of a deposition method under ambient conditions contributes for the research and characterization of these materials without requiring controlled atmosphere conditions.

In regard to the deposition optimization, the entire process from the substrate cleaning to the annealing was studied. Different types of annealing, spin parameters and solution configurations, anti-solvent washing methods were tested. An equal precursor ratio solution (1:1) of MAI and PbI_2 showed superior coverage when compared to a PbI_2 lower concentration solution used. The solvents tested were two mixtures of DMSO+GBL and DMF+DMSO. Both showed good coverage with a reduced number of pinholes, however, the DMSO+GBL film deposited showed uneven crystallization throughout the film (Figure 6), leading to the realization that using DMF+DMSO as solvents offered better results. The SiO_2 must be under ozone/UV treatment so that the perovskite film adheres to the substrate. However, over or under exposure to this treatment inhibits the film adhesion, through the studies made, 40 minutes of exposure is the ideal time for this substrate. A second step spin rate of 6000 rpm is also responsible for a better coverage and reduced number of pinholes.

The anti-solvent washing, and the annealing were essential steps in obtaining pinhole free films. Several different methods of anti-solvent washing, and annealing were tested. The most common method of dropping the anti-solvent during the spin-coating proved to be the most practical and optimal method. A volume of 200 μL produced better results, however, after further optimization of other steps like spin rate and annealing, a volume of 125 μL proved to be enough as the films showed good coverage, crystallization, and no pinholes. As for the annealing, options like the vacuum desiccator annealing and 2 step annealing had a strong influence on the film crystallization, helping to reduce pinholes and have good MAPI films. While these techniques were useful, it was still possible to achieve a pinhole free MAPI film with the regular hotplate annealing, with a temperature of 100 °C for 10 minutes. Furthermore, a use of more solution volume (125 μL) for the deposition also presented better films than using 80 μL. Through XRD measurements, final films have a bandgap of 1.59 eV, and it can be observed that there is a PbI_2 peak, indicating that not all the solvents reacted with the precursors.

The second goal of this work focused on the transistor fabrication and the electrical characterization of the perovskite material. The goal characterization of the deposited films was achieved allowing for the extraction of the mobility and polarization nature of the perovskite material. These devices, however, showed

poor performance under ambient conditions. At lower temperatures of 200K, the devices were more responsive. The mobility values are still below the best values reported in the literature.

Going forward, further studies on the relation of the MAPI films and the transistors made should be done. The films produced in this work showed good morphological characteristics yet that did not translate into a good electrical performance. There are other forces that influence the performance of a transistor besides the perovskite film like the interfaces with the contacts and the dielectrics, and so, a good film deposition does not guarantee that the transistor devices will have a good performance. Consequently, the devices may have performances that lead to a characterization of the MAPI mobility that does not reflect the inherent properties of the material. As such, further information, and research on the SiO_2 and MAPI interface is required to find the best deposition configuration. In addition, the use of other materials as a dielectric like Al_2O_3 to improve the interface with the perovskite material, helping to reduce the leakage current of the transistor devices. Moreover, additional electrical properties like the electrical resistivity, photoconductivity and carrier recombination should be studied to better understand and characterize the material employed.

REFERENCES

[1] W.-J. Yin, J.-H. Yang, J. Kang, Y. Yan, and S.-H. Wei, "Halide perovskite materials for solar cells: a theoretical review," *J Mater Chem A Mater*, vol. 3, no. 17, pp. 8926–8942, 2015, doi: 10.1039/C4TA05033A.

[2] B. A. Al-Asbahi, S. M. H. Qaid, M. Hezam, I. Bedja, H. M. Ghaithan, and A. S. Aldwayyan, "Effect of deposition method on the structural and optical properties of CH3NH3PbI3 perovskite thin films," *Opt Mater (Amst)*, vol. 103, p. 109836, May 2020, doi: 10.1016/j.optmat.2020.109836.

[3] T. Wu, W. Pisula, M. Y. A. Rashid, and P. Gao, "Application of Perovskite-Structured Materials in Field-Effect Transistors," *Adv Electron Mater*, vol. 5, no. 12, p. 1900444, Dec. 2019, doi: 10.1002/aelm.201900444.

[4] X. Zhao and N.-G. Park, "Stability Issues on Perovskite Solar Cells," *Photonics*, vol. 2, no. 4, pp. 1139–1151, Nov. 2015, doi: 10.3390/photonics2041139.

[5] Y. Syono, S. Akimoto, and K. Kohn, "Structure Relations of Hexagonal Perovskite-Like Compounds ABX $_3$ at High Pressure," *J Physical Soc Japan*, vol. 26, no. 4, pp. 993–999, Apr. 1969, doi: 10.1143/JPSJ.26.993.

[6] F. Paulus, C. Tyznik, O. D. Jurchescu, and Y. Vaynzof, "Switched-On: Progress, Challenges, and Opportunities in Metal Halide Perovskite Transistors," *Advanced Functional Materials*, vol. 31, no. 29. John Wiley and Sons Inc, Jul. 01, 2021. doi: 10.1002/adfm.202101029.

[7] M. Ye, X. Hong, F. Zhang, and X. Liu, "Recent advancements in perovskite solar cells: flexibility, stability and large scale," *J Mater Chem A Mater*, vol. 4, no. 18, pp. 6755–6771, 2016, doi: 10.1039/C5TA09661H.

[8] H. S. Jung and N.-G. Park, "Perovskite Solar Cells: From Materials to Devices," *Small*, vol. 11, no. 1, pp. 10–25, Jan. 2015, doi: 10.1002/smll.201402767.

[9] W.-J. Yin, T. Shi, and Y. Yan, "Unique Properties of Halide Perovskites as Possible Origins of the Superior Solar Cell Performance," *Advanced Materials*, vol. 26, no. 27, pp. 4653–4658, Jul. 2014, doi: 10.1002/adma.201306281.

[10] J. Wang *et al.*, "Investigation of Electrode Electrochemical Reactions in CH $_3$ NH $_3$ PbBr $_3$ Perovskite Single-Crystal Field-Effect Transistors," *Advanced Materials*, vol. 31, no. 35, p. 1902618, Aug. 2019, doi: 10.1002/adma.201902618.

[11] M. C. Gélvez-Rueda, M. B. Fridriksson, R. K. Dubey, W. F. Jager, W. van der Stam, and F. C. Grozema, "Overcoming the exciton binding energy in two-dimensional perovskite nanoplatelets by attachment of conjugated organic chromophores," *Nat Commun*, vol. 11, no. 1, p. 1901, Dec. 2020, doi: 10.1038/s41467-020-15869-7.

[12] C. Xie, C. Liu, H. Loi, and F. Yan, "Perovskite-Based Phototransistors and Hybrid Photodetectors," *Adv Funct Mater*, vol. 30, no. 20, p. 1903907, May 2020, doi: 10.1002/adfm.201903907.

[13] F. Zu, D. Shin, and N. Koch, "Electronic properties of metal halide perovskites and their interfaces: the basics," *Mater Horiz*, vol. 9, no. 1, pp. 17–24, 2022, doi: 10.1039/D1MH01106E.

[14] Y. Park and B. Park, "Interfacial energy band bending and carrier trapping at the vacuum-deposited MAPbI3 perovskite/gate dielectric interface," *Results Phys*, vol. 11, pp. 302–305, Dec. 2018, doi: 10.1016/j.rinp.2018.08.043.

[15] N. D. Canicoba *et al.*, “Halide Perovskite High- *k* Field Effect Transistors with Dynamically Reconfigurable Ambipolarity,” *ACS Mater Lett*, vol. 1, no. 6, pp. 633–640, Dec. 2019, doi: 10.1021/acsmaterialslett.9b00357.

[16] Y. Lin, P. Pattanasattayavong, and T. D. Anthopoulos, “Metal-Halide Perovskite Transistors for Printed Electronics: Challenges and Opportunities,” *Advanced Materials*, vol. 29, no. 46, p. 1702838, Dec. 2017, doi: 10.1002/adma.201702838.

[17] J. G. Labram *et al.*, “Temperature-Dependent Polarization in Field-Effect Transport and Photovoltaic Measurements of Methylammonium Lead Iodide,” *J Phys Chem Lett*, vol. 6, no. 18, pp. 3565–3571, Sep. 2015, doi: 10.1021/acs.jpclett.5b01669.

[18] C. A. Otálora, G. Gordillo, L. Herrera, and J. Estrada, “Effect of the solution chemistry on the film growth of hybrid MAPbI3 perovskites,” *Journal of Materials Science: Materials in Electronics*, vol. 32, no. 6, pp. 6912–6918, Mar. 2021, doi: 10.1007/s10854-021-05397-5.

[19] Mhd. I. Alturisa, J. Wira, Mardiyati, Herman, and R. Hidayat, “Influences of Precursor Solution Concentration and Temperature on $CH_3NH_3PbI_3$ Perovskite Layer Morphology and the Unconverted PbI_2 Proportion to their Perovskite Solar Cell Characteristics,” *J Phys Conf Ser*, vol. 877, p. 012046, Jul. 2017, doi: 10.1088/1742-6596/877/1/012046.

[20] S. Jana, E. Carlos, S. Panigrahi, R. Martins, and E. Fortunato, “Toward Stable Solution-Processed High-Mobility p - Type Thin Film Transistors Based on Halide Perovskites,” *ACS Nano*, vol. 14, no. 11, pp. 14790–14797, Nov. 2020, doi: 10.1021/acsnano.0c02862.

[21] J. R. Vig, “UV/ozone cleaning of surfaces,” *Journal of Vacuum Science & Technology A: Vacuum, Surfaces, and Films*, vol. 3, no. 3, pp. 1027–1034, May 1985, doi: 10.1116/1.573115.

[22] H. Baumg, / Irtner, V. Fuenzalida, and I. Eisele, “Applied so Ozone Cleaning of the Si-SiO 2 System,” 1987.

[23] Z. Zhou *et al.*, “The Effect of Annealing Pressure on Perovskite Films and Its Thin-Film Field-Effect Transistors’ Performance,” *physica status solidi (a)*, vol. 216, no. 22, p. 1900434, Nov. 2019, doi: 10.1002/pssa.201900434.

[24] M. Konstantakou, D. Perganti, P. Falaras, and T. Stergiopoulos, “Anti-Solvent Crystallization Strategies for Highly Efficient Perovskite Solar Cells,” *Crystals (Basel)*, vol. 7, no. 10, p. 291, Sep. 2017, doi: 10.3390/cryst7100291.

[25] S. Chen *et al.*, “Crystallization in one-step solution deposition of perovskite films: Upward or downward?,” *Sci Adv*, vol. 7, no. 4, Jan. 2021, doi: 10.1126/sciadv.abb2412.

[26] Y. Zhou *et al.*, “Manipulating Crystallization of Organolead Mixed-Halide Thin Films in Antisolvent Baths for Wide-Bandgap Perovskite Solar Cells,” *ACS Appl Mater Interfaces*, vol. 8, no. 3, pp. 2232–2237, Jan. 2016, doi: 10.1021/acsami.5b10987.

[27] L.-C. Chen, C.-C. Chen, J.-C. Chen, and C.-G. Wu, “Annealing effects on high-performance CH3NH3PbI3 perovskite solar cells prepared by solution-process,” *Solar Energy*, vol. 122, pp. 1047–1051, Dec. 2015, doi: 10.1016/j.solener.2015.10.019.

[28] Q.-Q. Ge *et al.*, “Promoting crystalline grain growth and healing pinholes by water vapor modulated post-annealing for enhancing the efficiency of planar perovskite solar cells,” *J Mater Chem A Mater*, vol. 4, no. 35, pp. 13458–13467, 2016, doi: 10.1039/C6TA05288F.

[29] L. Qin *et al.*, “Temperature dependent amplified spontaneous emission of vacuum annealed perovskite films,” *RSC Adv*, vol. 7, no. 26, pp. 15911–15916, 2017, doi: 10.1039/C7RA01155E.

[30] H.-L. Hsu, C.-P. Chen, J.-Y. Chang, Y.-Y. Yu, and Y.-K. Shen, "Two-step thermal annealing improves the morphology of spin-coated films for highly efficient perovskite hybrid photovoltaics," *Nanoscale*, vol. 6, no. 17, pp. 10281–10288, 2014, doi: 10.1039/C4NR02751E.

[31] *Physical Methods in Chemistry and Nano Science*.

[32] J. R. Albani, *Structure and dynamics of macromolecules : absorption and fluorescence studies*. 2004.

[33] F. Li *et al.*, "Ambipolar solution-processed hybrid perovskite phototransistors," *Nat Commun*, vol. 6, no. 1, p. 8238, Nov. 2015, doi: 10.1038/ncomms9238.

[34] H. P. Kim *et al.*, "A hysteresis-free perovskite transistor with exceptional stability through molecular cross-linking and amine-based surface passivation," *Nanoscale*, vol. 12, no. 14, pp. 7641–7650, 2020, doi: 10.1039/C9NR10745B.

[35] S. P. Senanayak *et al.*, "A general approach for hysteresis-free, operationally stable metal halide perovskite field-effect transistors," *Sci Adv*, vol. 6, no. 15, Apr. 2020, doi: 10.1126/sciadv.aaz4948.

2022 GUILHERME FERREIRA

OPTIMIZATION OF $MAPBI_3$-FILMS GROWN UNDER AMBIENT CONDITIONS ON SI/SIO_2 SUBSTRATES FOR ELECTRICAL CHARACTERIZATION OF PEROVSKITE MATERIALS

NOVA SCHOOL OF SCIENCE & TECHNOLOGY